SCHOLARONE™
Manuscripts

Accepted Article

This is the author manuscript accepted for publication and has undergone full peer review but has not been through the copyediting, typesetting, pagination and proofreading process, which may lead to differences between this version and the Version record. Please cite this article as doi:10.1002/lom3.10157.

This article is protected by copyright. All rights reserved.

SIPCO2: A simple, inexpensive surface water pCO_2 sensor

Christopher W. Hunt[1*], Lisle Snyder[2], Joseph E. Salisbury[1], Douglas Vandemark[1], William H. McDowell[2]

[1]Ocean Process Analysis Laboratory, University of New Hampshire, Durham, NH, USA

[2]Department of Natural Resources and the Environment, University of New Hampshire, Durham, NH USA

*corresponding author chunt@unh.edu (603) 862-1348

running head: Inexpensive DIY pCO_2 sensor evaluation

keywords: carbon dioxide, pCO_2, sensor, intercomparison, estuary, coastal

Accepted Article

This article is protected by copyright. All rights reserved.

Accepted Article

Abstract

Efforts to estimate air-water carbon dioxide (CO_2) exchange on regional or global scales are constrained by a lack of direct, continuous surface water CO_2 observations. Sensor technology for the in-situ measurement of the partial pressure of carbon dioxide (pCO_2) has progressed, but still poses limitations including expense and biofouling concerns. We describe a simple, inexpensive, in-situ pCO_2 method (SIPCO2) in which a non-dispersive infrared (NDIR) detector is paired with an air pump in an enclosed housing to produce air-sea equilibration. We first evaluated this approach in a laboratory setting, then in an estuarine-coastal ocean laboratory for several months to continuously monitor aquatic pCO_2. An accepted, accurate NDIR-based CO_2 measurement technique was employed alongside SIPCO2 to provide an assessment of sensor performance. SIPCO2 allows for low-cost, relatively accurate measurements of pCO_2 (mean difference of -5 ±5 µatm from validation system after laboratory calibration) without reagents or membranes, and can be assembled and operated with a minimal amount of technical skill. While not suitable for some exacting applications, this SIPCO2 approach could rapidly and effectively increase the number of quality CO_2 observations in a range of aquatic environments. We also provide detailed instructions for the assembly of SIPCO2 from commercially available components.

Introduction

Recent examinations of the fluxes of carbon dioxide (CO_2) between the terrestrial, atmospheric, inland aquatic, estuary, and coastal ocean provinces have illustrated both their

This article is protected by copyright. All rights reserved.

dynamic nature and importance to regional and global carbon budgets (Frankignoulle 1988, Raymond et al. 1997, Cole et al. 2007, Signorini et al. 2013, Raymond et al. 2013, Laruelle et al. 2014, Laruelle et al. 2015, Borges et al. 2015). Many of these studies, particularly those focused on inland waters, have not used direct observations of the partial pressure of carbon dioxide (pCO_2) in water, but instead have derived pCO_2 from other measures of the carbonate system for some or all of the analysis (Raymond et al. 1997, Cole et al. 2007, Atilla et al. 2011, Butman and Raymond 2011, McDonald et al. 2013, Laruelle et al. 2015). This derivation is commonly accomplished through the pairing of discrete total alkalinity and pH sample data (Park 1969), a technique which has been shown to result in a large potential overestimate of pCO_2 due to diverse factors such as interferences (particularly in freshwater systems) from non-carbonate contributions to alkalinity (Hunt et al. 2011, Wang et al. 2013, Abril et al. 2015) and electrode-based pH measurement errors in seawater (Hoppe et al. 2012, Bockmon and Dickson 2015).

While a more complete understanding of non-carbonate contributions to alkalinity could potentially lead to accurate indirect estimates of pCO_2 from discrete measurements- as could the pairing of sample measurements of dissolved inorganic carbon and pH- an alternative way to improve and constrain CO_2 budgets is to vastly increase the number of direct pCO_2 observations, especially in freshwaters where non-carbonate interferences are the most prevalent. The need for direct pCO_2 measurements, together with technological improvements, has resulted in a variety of innovative new pCO_2 sensor technologies. These technologies employ several equilibration techniques, including headspace equilibration through a gas-permeable membrane and non-membrane equilibration, as well as contrasting CO_2 detection techniques such as non-dispersive infrared (NDIR) detection and chemical reagent detection (Table 1). An evaluation of four commercial pCO_2 sensors in coastal waters by the Alliance for Coastal Technology in 2010

Accepted Article

This article is protected by copyright. All rights reserved.

found a range of sensor performance compared to a documented underway-type pCO_2 system (using a membrane-based equilibrator and NDIR CO_2 detection, Hales and Takahashi 2004) and discrete pCO_2 measurements (pCO_2 derived from total alkalinity and pH). A separate evaluation of a membrane-equilibration technique compared sensor data to discrete headspace CO_2 measurements with a large range of reported sensor discrepancy (Johnson et al. 2010).

Although these commercial in-water measurement sensors are generally pre-configured for immediate use, they are also vulnerable to biofouling (especially in the case of membrane-type systems and the SAMI-CO_2 water intake tube), are sometimes complex to install due to multiple components requiring specialized mounting hardware (MAPCO2), and costly. Recently, Bastviken et al. (2015) presented a innovative design for a passively equilibrated pCO_2 sensor, using the same low-cost CO_2 detector employed in this study, with good detector linearity and promising results against discrete bottle-headspace pCO_2 measurements. These results indicate that these inexpensive detectors hold great potential for the construction of an *in* situ *p*CO2 sensor. However, the bottle-headspace method has several shortcomings (Bastviken et al. 2015), and that study did not provide assessment of performance against a validated continuous headspace-equilibration system. Here we present an alternative design for a simple, inexpensive pCO_2 sensor (SIPCO2) that can be assembled in a few hours from off-the-shelf or easily obtained components totaling less than $500 USD. We then present results from two evaluation exercises, the first a multi-day lab test in a tank of manipulated freshwater, the second a multi-month test at a coastal laboratory. While we emphasize and discuss how evaluation conditions differed between the SIPCO2 evaluations and those of commercially available sensors, and thus results may not be directly comparable, SIPCO2 performance was similar to

Accepted Article

This article is protected by copyright. All rights reserved.

that of the sensors listed in Table 1 once calibrated against an accepted pCO_2 measurement system.

Accepted Article

Materials and Procedures

Equilibration background

Among all styles of in-water CO_2 sensors, one common element is the necessity to separate aqueous CO_2 from the liquid medium into a measureable state. All the sensors in Table 1 measure CO_2 in the gaseous state via NDIR detection with the exception of the Sunburst SAMI-CO_2, which measures pH change in the liquid phase as CO_2 exchanges across a membrane (DeGrandpre et al. 1995). In marine pCO_2 observations the technique of equilibrating an air headspace with a water mass of interest has been used for decades (Takahashi 1961, Weiss 1981, Wanninkhof and Thoning 1993). According to this technique, after equilibration the gas composition of the headspace reflects that of the water mass. Often the equilibrator is a showerhead-type in which the air headspace is ultimately pumped to a NDIR detector at a set rate. The MAPCO2 system achieves equilibration through a combination of wave and bubble action, and components in contact with seawater are constructed of copper alloy to prevent biofouling (Friederich et al. 1995, ACT 2010d). All types of equilibrators can be vulnerable to fouling, even those constructed using an anti-fouling agent such a copper, and must be cleaned often to maintain accurate pCO_2 measurements. More recently, use of this technique has migrated upstream to estuary and freshwater environments (Frankignouelle and Borges 2001, Abril et al. 2006). The underlying principle of this type of equilibration requires that a relatively large volume of water is exchanged with a relatively small air headspace to equilibrate the CO_2

This article is protected by copyright. All rights reserved.

levels between the two media. This concept requires the transfer via pumps of small volumes of air and larger volumes of water. Our design simplifies this concept by re-circulating headspace air below the water surface via a small air pump; the resulting bubbles equilibrate CO_2 with the surrounding water, break, and the released air rises through tubing or a pipe back to the headspace containing a small NDIR detector (Figure 1). The same headspace air is re-circulated, providing equilibration at a rate suitable for applications where: a) the sample water is not rapidly changing its carbonate characteristics, and b) bubbles do not escape the return pipe or the enclosure is not opened to ambient air.

SIPCO2 Sensor Design

The SIPCO2 sensor design (Figure 1) has two electro-mechanical components- the air pump and NDIR detector- housed in an off-the-shelf plastic electrical junction box (component parts list included in Supplementary Material). In order to maintain equilibration, the air pump is run continuously, although it may be possible to run the pump intermittently to conserve power, especially when powered by a battery. The flow rate of the selected pump is listed by the manufacturer (KNF Neuberger) as 0.45 l min^{-1}, with an operating life of 10,000 hours for the brushless model, although in other applications we have observed pump durability of 4-5 years.

The NDIR detector employed in this work was a SenseAir K-30 (ASCII model, SenseAir AB, Delsbo Sweden). The K-30 detector has a manufacturer-specified measurement range of 0-10,000 ppm CO_2, an accuracy of ± 30 ppm ± 3 % of the measurement value, and a precision of ± 20 ppm ± 1 % of the measurement value. Our own results found that with calibration the K-30 can achieve both better accuracy and better precision, as discussed below. The ASCII output version of the K-30 sensor used in this work provides an automatic ASCII-format CO_2

Accepted Article

This article is protected by copyright. All rights reserved.

measurement every two seconds. A vendor-supplied control program ("Gaslab") was used to calibrate the K-30, although this program is limited to calibration concentrations of 0 and 400 ppm only. For both the Laboratory Evaluation and Coastal Laboratory Evaluation discussed below, the SIPCO2 sensor was powered by a standard 5-volt Universal Serial Bus connection to a laptop computer. This computer also logged the ASCII SIPCO2 data output via a terminal program. The K-30 comes equipped with an onboard temperature sensor. While we performed a later evaluation of the temperature dependency of the K-30 (described below), the onboard temperature component failed during the two central evaluations of this work.

Validation System

The validation system, typically used for shipboard continuous-flow pCO_2 measurements (see Hunt et al. 2013) consisted of an equilibrator with spray nozzle, with headspace air recirculated by a small air pump between the equilibrator and a Li-cor LI-840 NDIR detector. The manufacturer-specified operating range of the LI-840 NDIR is 0-3000 ppm CO_2. The validation system was calibrated with ultrapure nitrogen and an 835 ppm CO_2/nitrogen mixture, and a computer-controlled system of valves flowed the same calibration gases through the validation LI-840 NDIR once every three hours to check system calibration stability. The estimated uncertainty of the validation system is +/- 3 µatm (Vandemark et al. 2011).

pCO_2 Calculation

The SIPCO2 K-30 detector reported measurements as the molar fraction of CO_2 (xCO_2). Since the sensor housing was open to the water surface, the readings reported by the SIPCO2 sensor were 'wet' (xCO_{2wet}). These xCO_{2wet} data were corrected to sea surface temperature,

This article is protected by copyright. All rights reserved.

assuming the temperature inside the SIPCO2 was also equilibrated to the observed sea surface temperature, and converted from xCO_{2wet} to the partial pressure of carbon dioxide (pCO_2, wet air), according to standard methods (Dickson et al. 2007), assuming the SIPCO2 headspace was at ambient atmospheric pressure, measured by a nearby meteorological array. In contrast, the sample stream of the validation system described below was drawn through tubing containing a Nafion selectively permeable membrane (Perma Pure, Toms River NJ), which dried the sample gas stream of water vapor, resulting in validation system readings of xCO_{2dry}. These xCO_{2dry} validation data were corrected to sea surface temperature and converted from xCO_{2dry} to pCO_2 as above (Dickson et al. 2007). Thus, all pCO_2 data presented in this work are in the form of partial pressures of CO_2 in wet air.

Laboratory Evaluation

The K-30 detector was initially removed from the SIPCO2 housing and calibrated in the lab by placing the sensor in a sealed plastic bag with a small opening for gas tubing and detector cable. When gas flow was introduced the positive pressure flushed the bag after several minutes, allowing for stable CO_2 readings from the detector. The detector was zeroed with ultrapure nitrogen, then subsequently spanned with a 400 ppm CO_2/nitrogen mixture. The limitations of this detector calibration procedure are discussed later in this work. After calibration, the K-30 detector was placed into the sensor housing and run in the lab continuously for several days alongside a more traditional aquatic CO_2 system. Both pCO_2 systems measured a tank of ~200 l tap water, with the SIPCO2 sensor placed directly into the tank, while water was recirculated between the tank and validation system's equilibrator via a submersible pump. The temperature of the SIPCO2 headspace was assumed to be equal to that of the water in the tank. The

Accepted Article

This article is protected by copyright. All rights reserved.

simultaneous use of the SIPCO2 and validation systems allowed us to compare the behavior of the SIPCO2 sensor over a wider range of CO_2 in the lab, as carbonated water was added to the tank twice to raise CO_2 levels (Figure 2). These carbonated water additions also allowed the estimation of the SIPCO2 sensor response time.

Coastal Marine Laboratory Evaluation (CML)

A longer-term sensor evaluation was conducted from November 22, 2014 to March 12, 2015 at the University of New Hampshire Coastal Marine Laboratory (CML), a facility at the mouth of the Piscataqua River, which drains to the coastal Gulf of Maine (43.0°N 70.7°W). The facility has a continuous seawater supply, pumped from near the bottom of the adjacent channel at a tide-varying depth between 4.5-7 m. The same sensor used in the laboratory evaluation , which was not recalibrated following the laboratory evaluation, was placed into a ~200 l tank similar to that used in the laboratory evaluation, which was continuously flushed with seawater at an approximate rate of 10 l/min. The CML tank also contained a thermosalinograph (Aanderaa 4319B), which collected data for 10 minutes each hour. Salinities reported in this paper are on the PSS-78 scale (Lewis 1980). A separate seawater line continually supplied the headspace gas equilibrator for the CML CO_2 seawater measurement system. This system was identical to that used in the laboratory evaluation, and measurements of ultrapure nitrogen and an 835 ppm CO_2/nitrogen mixture were made every four hours to determine the stability of the validation system. While the SIPCO2 and validation CO_2 systems were run continuously, only the pCO_2 data from these systems collected over the ten-minute period when the thermosalinograph was in operation were used to produce 10-minute average values once per hour, which comprise the dataset presented here.

Accepted Article

This article is protected by copyright. All rights reserved.

Assessment

Laboratory Evaluation

During the laboratory evaluation the SIPCO2 sensor closely tracked the validation system during unperturbed periods (r^2=0.99). Shortly after two rapid additions of CO_2 the SIPCO2 sensor response lagged that of the validation system (Figure 2). Results of mean offsets (Off_{mean}, calculated as differences between sensor readings, Equation 1) show that readings from the SIPCO2 sensor were consistently higher than those from the validation system (excepting the periods of rapid CO_2 increase during the two perturbation periods). This consistent offset was present despite the calibration of the SIPCO2 NDIR detector with the same gas standards used to calibrate the validation system (Table 2).

$$Off_{mean} = \frac{1}{n} * \sum_{i=1}^{n} (pCO_{2\,SIPCO2} - pCO_{2\,Validation}) \quad (1)$$

There is a substantial discrepancy between the mean offsets if data from the perturbation periods are included (Table 2). Standard deviations of the mean offsets (calculated as in Equation 2) show that the perturbation periods represented a large amount of variance, while ignoring these periods yielded a standard deviation (precision) of ±14 µatm. A ±14 µatm precision, which translates to a ±3.5% relative uncertainty at a pCO_2 of 400 µatm, represents an unacceptable level of uncertainty for exacting applications; for instance, this uncertainty exceeds the desired levels of both the 'weather' and 'climate' objectives (2.5% and 0.5% desired

Accepted Article

This article is protected by copyright. All rights reserved.

uncertainty, respectively) of the Global Ocean Acidification Observing Network (GOA-ON, Newton et al. 2015).

$$Off_{std} = \sqrt{\frac{1}{n}\sum_{i=1}^{n}(pCO_{2\,SIPCO2} - pCO_{2\,Validation})^2} \quad (2)$$

Linear regressions of the SIPCO2 sensor readings against those from the validation system, both for the entire comparison period and for the two periods without CO_2 additions are listed in Table 2. The response time of the SIPCO2 system lagged that of the validation system, resulting in the separation of the two peaks in Figure 2 (top panel) and deviation from linearity apparent in Figure 2 (bottom panel). The time lag between the highest validation system pCO_2 and SIPCO2 pCO_2 was approximately nine minutes for the first peak, and 11 minutes for the second peak, indicating a slower response time for the SIPCO2 sensor. The validation system responded quickly to the CO_2 additions (less than one minute from initial addition to the start of the validation system response), while three and four minutes elapsed between the start of the validation response to peak validation pCO_2), resulting in total validation system response times of four and five minutes for the first and second peaks, respectively. Addition of these validation system response times with the nine and 11 minute lags between the validation and SIPCO2 peaks, together with a one minute lag between the CO_2 addition and start of validation system response, results in a conservative SIPCO2 response time estimate of 15 minutes. The highest SIPCO2 readings for the two peaks (1284 and 1421 µatm, respectively) were lower than those from the validation system (1411 and 1618 µatm, respectively), suggesting that the added CO_2 from the carbonated water escaped the tank quickly enough that the SIPCO2 sensor could not fully equilibrate due to the slower SIPCO2 sensor response time. This is probably due in part to

Accepted Article

This article is protected by copyright. All rights reserved.

the rapid recirculation of water through the validation system's equilibrator; thus, we might expect a slower CO_2 decrease in naturally less-turbulent waters.

We performed a linear regression of the SIPCO2 sensor readings against those from the validation system according to Equation 3, to examine the linear response of the SIPCO2 sensor (Table 2, Figure 2). When the peaks from the CO_2 additions were excluded, the SIPCO2 sensor response was quite linear to that of the validation system (r^2=0.99), with a near 1:1 slope.

Coastal Marine Laboratory Evaluation

Hydrographic conditions at the CML varied over the approximately three and a half months the SIPCO2 sensor was deployed (Table 3). Water temperatures gradually decreased from 10°C to near 0°C as the season progressed from late fall to winter, then began to rise at the end of the evaluation in spring. Salinity reached a minimum in late December due to higher than normal rainfall. Underlying these seasonal changes were clear semi-diurnal tidal signals, with high tide bringing warmer water temperatures and higher salinities. The magnitudes of salinity and temperature changes varied with lunar phase, as well as with precipitation and associated changes in freshwater input, but water temperature generally varied 1-2°C between low and high tides, while salinity varied 1.5-3.

As in the laboratory evaluation, the SIPCO2 sensor sensitively tracked the readings of the validation pCO_2 system at the CML, but with somewhat higher readings (Figure 3, Tables 2 and 4). The offset between the SIPCO2 sensor and validation system (Figure 3, bottom panel) varied from 7 to 65 µatm over the CML test, with a mean offset of 29 µatm and standard deviation of 6 µatm (Table 4). This mean offset from the CML evaluation is somewhat lower than the mean offset found in the laboratory evaluation (42.7 µatm, without peaks), but within

Accepted Article

This article is protected by copyright. All rights reserved.

one standard deviation of the laboratory evaluation mean (Table 2). Paired t-tests show that the mean CML offset is significantly different than the mean Laboratory Evaluation offset at the 95% significance level. The results of a linear regression of the SIPCO2 readings against those from the validation system at the CML yielded slightly different slopes than observed in the laboratory evaluation (1.08 and 1.03 µatm, respectively), as well as different intercepts (-1.9 and 22 µatm, respectively).

Coastal Marine Laboratory Evaluation Data Correction

We used the results of the laboratory evaluation results in two ways to attempt to correct the SIPCO2 sensor readings at the CML site. First, we used a simple offset removal, subtracting 42.7 µatm from the SIPCO2 sensor readings at the CML (Table 4). This offset correction lowered the mean CML offset to -13.8±6 µatm, which is closer to an ideal offset of 0 µatm. Second, we used the results of the linear regression of the laboratory evaluation and applied the same slope and intercept to the CML SIPCO2 sensor data (Table 4), according to Equation 3:

$$pCO_{2\,corrected} = \frac{(\mathrm{pCO_{2\,SIPCO_2}} - 22)}{1.03} \quad (3)$$

This simple application of the slope and intercept from linear regression of the Laboratory Evaluation data produced the best SIPCO2 results from the CML (Figure 4), bringing the mean offset to -5±5 µatm.

Discussion

Accepted Article

This article is protected by copyright. All rights reserved.

For many pCO_2 measurement applications in estuaries, lakes, or rivers, a SIPCO2 accuracy and precision of 29±6 µatm, as determined in the CML evaluation, or 42.7±14.2 µatm in the case of the laboratory evaluation, may be acceptable for examinations of air-water CO_2 fluxes or aquatic ecosystem metabolism; however, it is important to acknowledge that pCO_2 levels and range of variation in freshwater and estuary systems can be several times to an order of magnitude larger than the range tested in the CML evaluation. For instance, Abril et al. (2006) showed precision of directly measured river pCO_2 of ±15% over a 0-13,000 ppm range. Borges et al. (2015) documented a method precision of ±2% for IRGA-based direct measurements of African rivers ranging in pCO_2 from 300-16,942 ppm. Hanson et al. (2003) determined net ecosystem productivity via IRGA-based pCO_2 measurements in 25 lakes, with an estimated pCO_2 precision of ±2% over a 0-20,000 ppm range. Raymond et al. (1997) showed a precision of ±8% over a range of about 500-2000 ppm in the tidal Hudson River estuary. Although the SIPCO2 level of accuracy and precision may be unacceptable for "climate" quality oceanic studies, the precision of results from the CML evaluation (±6 µatm) exceeds the 'weather' target uncertainty of ±10 µatm (±2.5% at 400 µatm pCO_2), but falls short of the 'climate' target uncertainty of ±2 µatm (±0.5% at 400 µatm pCO_2, Newton et al. 2015). Furthermore, we have found that a pre- (and perhaps post-) deployment laboratory calibration may offer a way to improve the data quality from the SIPCO2 sensor.

We anticipate that a longer laboratory evaluation period with larger and more gradual pCO_2 changes than shown here will produce a more robust regression calibration. Thus, while a simple offset subtraction improved the SIPCO2 sensor readings at the CML site, the generation of a linear regression relationship against readings from a validation system appears to be a reasonable way to correct readings from this SIPCO2 sensor. It is worth noting that the CML

Accepted Article

This article is protected by copyright. All rights reserved.

evaluation spanned pCO_2 levels of a fairly narrow range (340-500 µatm). Freshwater field evaluations and verification of the linearity of the SIPCO2 sensor response are presently underway. Preliminary results indicate that the SIPCO2 sensor works well in the elevated pCO2 environment found in local rivers, where a wider range of pCO_2 is expected. This is consistent with the K-30 measurement specifications of Bastviken et al. (2015). The results of Bastviken et al. (2015) indicate that corrections for detector temperature and relative humidity offer additional ways to improve the quality of CO_2 readings from the K-30 NDIR detector, but we expect humidity impacts to be low for the SIPCO2 sensor due to typical operation at ~100% humidity in continuous mode. While Bastviken et al. (2015) noted problems with condensation, no condensation was observed in the SIPCO2 housing during these tests.

Potential Sources of Error and Uncertainty

The consistent presence of an offset between SIPCO2 readings and those of the validation pCO_2 system (+42.7 µatm in the laboratory evaluation , Table 2, and +29 µatm in the CML test, Table 4) suggest that there are additional sources of error in the SIPCO2 system. If quantified, knowledge of these errors could be used to improve the SIPCO2 data quality. Due to its simple design, the SIPCO2 system has two components which can create potential sources of error: the air pump and the K-30 NDIR detector. Faults in the air pump would result in incomplete equilibration or slower response times. While the response of the SIPCO2 lags that of the validation system (Figure 2), an increase in this lag on the order of minutes may have produced a smaller offset, as shown by the difference between the Off_{mean} values with and without peaks shown in Table 2. The air pump used in both the Laboratory and CML evaluations was not observed to have failed or exhibited reduced flow rates.

Accepted Article

This article is protected by copyright. All rights reserved.

The K-30 NDIR detector is a more likely source of error in the SIPCO2 design. We performed three tests on a new K-30 NDIR sensor: linearity of response, temperature response, and humidity response. This K-30 module was not the same as used in the Laboratory and Coastal Laboratory evaluations, but was the same model and was prepared and calibrated with UHP N_2 and 400 ppm CO_2 in the same manner as described above. Similar to Bastviken et al. (2015), we compared the response of the K-30 NDIR to that of a Li-cor LI-840 NDIR, the same highly linear model used in the laboratory and CML evaluations of the SIPCO2 sensor. This response test was performed by mixing streams of ultrapure nitrogen and pure CO_2 with a valve to produce mixtures from 0 ppm to near-10,000 ppm CO_2, then flowing the mixed gas stream sequentially through the LI-840 and K-30 NDIR detectors, which were connected by short lengths of tubing. Results of this linearity test show that the response of the K-30 NDIR is linear (r^2=0.9998, Figure 5). However, the slope of the regression line between K-30 and LI-840 NDIR detectors indicates that the K-30 NDIR underestimates xCO_2 at higher concentrations (slope=0.93). This is a somewhat different finding than that presented by Bastviken et al. (2015), which showed a linear response from the K-30 NDIR but used a comparison NDIR (Los Gatos Research DLT100) that exhibits quenching effects and nonlinear behavior at higher CO_2 concentrations. At 350 µatm pCO_2, the approximate minimum reading during the CML evaluation, this translates to an offset of -26 µatm (calculated according to Equation 1), while at 500 µatm pCO_2 the calculated offset is -36 µatm. The fact that this response linearity offset is negative (i.e. LI-840 readings are higher than K-30 readings), while the overall Off_{mean} results from the Laboratory and CML evaluations were positive indicates that another factor was more than offsetting the differences in response linearity between the two NDIR detectors. This finding indicates that calibration of a K-30 NDIR with mixtures of gases may not be sufficient to

Accepted Article

This article is protected by copyright. All rights reserved.

quantify the overall performance of a SIPCO2 sensor, and comparison to a validation system such as the one discussed here is advisable for highly accurate results.

Other studies examining the K-30 NDIR have demonstrated that the detector is sensitive to temperature and humidity changes (Bastviken et al. 2015, Yasuda et al. 2012). To examine the temperature response of the K-30 NDIR, we first calibrated the sensor at 20°C using ultra-high purity (UHP) nitrogen and 400 ppm CO_2 in nitrogen. We then flowed either UHP nitrogen or a 515 ppm mixture of CO_2 in nitrogen through the K-30 NDIR while altering the temperature of the K-30 detector. The temperature was altered by placing the K-30 NDIR was on a chilled laboratory hot plate, which has previously been kept in a freezer. Contact between the K-30 NDIR and the chilled hot plate lowered the temperature of the K-30 to 5-10°C; the hot plate was then slowly warmed to 30-50°C, and the xCO_2 response of the K-30 NDIR was recorded (Figure 6). The change in xCO_2 reading from temperature change was nearly identical between UHP nitrogen and 515 ppm CO_2. xCO_2 readings from the K-30 NDIR increased at temperatures greater than the calibration temperature (20°C), and fell below the known gas concentration at temperatures less than 20°C.

The K-30 NDIR has an onboard temperature sensor, and provides a detector temperature reading as part of its typical data stream. This offers the potential opportunity to temperature-correct the xCO_2 readings from a K-30 NDIR, using the logarithmic regression equation presented in Figure 6. While Bastviken et al. (2015) noted a lack of temperature effect on K-30 readings, the equation shown in Figure 6 is quite similar to the linear correction presented in Yasuda et al. (2012), a study in which several identical K-30 sensors were evaluated simultaneously.

Accepted Article

This article is protected by copyright. All rights reserved.

To test the effect of varying humidity on K-30 NDIR readings, we employed a Li-cor 610 portable dew point generator. UHP nitrogen and the same 514 ppm CO_2 mixture employed above were flowed through the LI-610 instrument set to a dew point of 0°C, then subsequently to the K-30 NDIR sensor. The LI-610 was then adjusted to gradually increase the dew point of the UHP nitrogen or 514 ppm CO_2 mixture, while readings from the K-30 sensor were recorded. This test showed increasing xCO_2 readings from the K-30 sensor for UHP nitrogen, while the 514 ppm CO_2 mixture showed an initial slight xCO_2 decrease, followed by an xCO_2 increase above a dew point of about 10°C (Figure 7). The temperature of the K-30 NDIR did not change appreciably over either dew point test, indicating that changes in xCO_2 readings were due solely to humidity. The manufacturer of the K-30 NDIR also offers models with onboard relative humidity measurements (i.e. K-33 ELG), the use of which offer the potential to correct for both temperature and humidity effects. While these models are somewhat more expensive, the capability to perform both temperature and humidity corrections would likely be valuable, particularly if the SIPCO2 sensor is to be deployed outside under a wide range of environmental conditions.

In light of these error sources, we can speculate whether some combination of the systematic K-30 underestimate of xCO_2 (Figure 5), temperature effects (Figure 6), and humidity effects (Figure 7) can explain much of the Off_{mean} determined in both the Laboratory and CML evaluations (Tables 2 and 4). Unfortunately, the temperature detector in the SIPCO2 K-30 used in both laboratory and CML evaluations malfunctioned, making post-correction of the data impossible. However, we can estimate what the potential effects would be at some likely temperatures, with a few assumptions. First, we assume that the air inside the SIPCO2 was at 100% humidity, as it was constantly recirculated beneath the water's surface by the air pump

Accepted Article

This article is protected by copyright. All rights reserved.

while remaining isolated from surrounding ambient air. Second, both the laboratory and CML evaluations were performed inside temperature-controlled buildings (although the CML building was generally colder), so we assume the air temperature inside the SIPCO2 was between 15-25°C. Given these assumptions, the contribution of humidity to the observed Off_{mean} should have been small (0 µatm at 15°C to 5 µatm at 25°C). Similarly the temperature contribution to the observed Off_{mean} should also have been small (-8 µatm at 15°C to 5 µatm at 25°C, given a K-30 calibration temperature of 20°C). As previously discussed, at the minimum CML evaluation pCO_2 of 350 µatm the linearity offset is -26 µatm (calculated according to Equation 1), while at 500 µatm pCO_2 the offset is -36 µatm. Combining linearity and humidity errors yields a net error offset ranging from -44 µatm (at 15°C and 500 µatm) to -16 µatm (at 25°C and 350 µatm). Under the above assumptions, the detector temperature would have to be 183°C to account for the linearity error, humidity error, and observed Off_{mean} at 350 µatm, while the temperature would have to be 284°C to account for the same errors at 500 µatm. These results indicate that factors other than linearity, temperature, and humidity are producing the observed Off_{mean}; the results also underscore the importance of a careful evaluation of a SIPCO2 system against a validation system before attempting to make accurate measurements.

Comparison to other pCO_2 sensors

The pCO_2 readings from the SIPCO2 sensor before post-deployment adjustment underperformed some commercial sensors. For example, Degrandpre et al. (1995) demonstrate a SAMI-CO_2 accuracy/precision of ±2 µatm and ±1 µatm, respectively, although an intercomparison with a NDIR-based equilibrator system resulted in an overall offset between the two systems of 3.7 µatm. In comparison to a NDIR-based equilibrator system, Fietzek et al.

Accepted Article

This article is protected by copyright. All rights reserved.

(2013) found a Contros Hydro-C offset and precision of -0.6 µatm and ±3 µatm, respectively. However, after careful characterization against a validation system the SIPCO2 sensor performance is comparable to that of some of the systems presented in Table 1. The sensors discussed in the ACT evaluations: Contros Hydro-C (Fietzek et al. 2013), Pro-Oceanus CO_2-Pro, Sunburst SAMI-CO_2 (Degrandpre et al. 1995), and PMEL/Batelle MAPCO2 (Friederich et al. 1995) were tightly restricted, while we had continuous access to the SIPCO2 system, so this work does not present an evaluation conducted under directly comparable conditions to many of the sensors listed in Table 1.

The presented SIPCO2 sensor configuration ($200USD to $500USD for sensor components, see Supplementary Material) offers a significant price advantage in comparison to the commercial systems described in Table 1. One disadvantage of the SIPCO2 sensor is an assembly time of several hours combined with a further time requirement to evaluate sensor performance, as opposed to an off-the-shelf system. However, we also believe the SIPCO2 configuration, using a small air pump to recirculate air within a small housing, offers a reduced risk of biofouling or sensor damage when compared to sensors that employ a membrane to exchange CO_2. Another advantage of the SIPCO2 design is the modular nature of the sensor, which allows for the easy replacement of components that may fail over time.

One disadvantage of the SIPCO2 sensor as described here is its response time, which is somewhat slow in comparison to other commercial sensors (on the order of ten minutes in the laboratory evaluation). The use of a more powerful air pump to provide a higher flow rate should mitigate this issue, although we have not tested this possibility. The results in this work suggest that the SIPCO2 sensor could support many fixed-location scientific and monitoring applications, as opposed to use as a portable handheld pCO_2 sensor such as described in Johnson

Accepted Article

This article is protected by copyright. All rights reserved.

et al. (2010). Interestingly, Bastviken et al. (2015) show a negligible difference in pCO_2 readings between pumped and unpumped systems, although their measurement timescale was on the order of several hours. Further investigation into response time and mixing rates is warranted depending on specific application needs.

A key issue in the use of the SIPCO2 sensor relates to calibration. The host software for the K-30 CO_2 detector used in the SIPCO2 sensor at present only allows calibrations with gases of zero and 400 ppm CO_2. This is a relatively narrow calibration range for many applications, as pCO_2 can range an order of magnitude or higher in aquatic systems (Raymond et al. 1997, Hunt et al. 2013, Bastviken et al. 2015). While Bastviken et al. (2015) and results in this work show good K-30 sensor linearity, this limited K-30 calibration range underscores the need to characterize the SIPCO2 system against a validation system in a variety of environments.

Because the SIPCO2 sensor housing is not completely sealed from the environment, the present design is not submersible, and thus is only useful for surface measurements or integrated measurements of pCO_2 down to the depth of the pump's air tubing. Furthermore, this version has no ability to log data internally or operate autonomously on battery power. However, the cost, ease of assembly, and quality of data suggest that the SIPCO2 provides a potentially valuable instrument for observation nodes in freshwater, estuary, and coastal environments. The addition of low-cost components could readily address data-logging and power issues. The SIPCO2 sensor represents a basic platform for aquatic pCO_2 measurements, to which users could add functionality to suit individual needs and requirements.

Comments and Recommendations

Accepted Article

This article is protected by copyright. All rights reserved.

This paper presents a new design for a relatively inexpensive sensor to measure aquatic pCO_2 from readily obtainable components, evaluates the performance of the sensor in two settings, and provides a simple method to correct the sensor data against a known validation system. Uncorrected SIPCO2 sensor performance is below that of comparable commercial sensors (30±6 µatm difference from validation system), but post-deployment correction of the SIPCO2 measurements produces data of comparable quality (-5 ±5 µatm difference from validation system).

While many researchers may prefer out-of-the-box sensors for their application, we expect that the open design and cost savings of the SIPCO2 sensor will make it appealing to many users. The supplementary material provides a list of SIPCO2 sensor components, suppliers for many of the components, as well as step-by-step instructions for assembly. We strongly recommend calibration of the SIPCO2 sensor against a known validation system in order to produce the highest quality data possible. One potentially powerful use of this sensor is within a network of observation nodes, where numerous sensors could be deployed spatially around a validation system. This could dramatically increase the extent of in-situ pCO_2 coverage while assuring data quality using a single expensive validation system.

Accepted Article

This article is protected by copyright. All rights reserved.

References

Abril, G., S. Richard, and F. Guérin. 2006. In situ measurements of dissolved gases (CO2 and CH4) in a wide range of concentrations in a tropical reservoir using an equilibrator. Science of The Total Environment 354: 246–251.

Abril, G., S. Bouillon, F. Darchambeau, C. R. Teodoru, T. R. Marwick, F. Tamooh, F. Ochieng Omengo, N. Geeraert, L. Deirmendjian, P. Polsenaere, and A. V. Borges. 2015. Technical Note: Large overestimation of pCO2 calculated from pH and alkalinity in acidic, organic-rich freshwaters. Biogeosciences 12: 67–78.

Alliance for Coastal Technologies, 2010a. Performance Demonstration Statement for Contros HydroC™/CO2, ACT DS10-01 UMCES/CBL 10-091.

Alliance for Coastal Technologies, 2010b. Performance Demonstration Statement for Pro-Oceanus Systems Inc. PSI CO_2-Pro™, ACT DS10-03 UMCES/CBL 10-093.

Alliance for Coastal Technologies, 2010c. Performance Demonstration Statement for Sunburst Sensors SAMI-CO_2, ACT DS10-04 UMCES/CBL 10-094.

Alliance for Coastal Technologies, 2010d. Performance Demonstration Statement for PMEL MAPCO_2/Battelle Seaology pCO_2 Monitoring System, ACT DS10-02 UMCES/CBL 10-092.

Accepted Article

This article is protected by copyright. All rights reserved.

Atilla, N., G. A. McKinley, V. Bennington, M. Baehr, N. Urban, M. DeGrandpre, A. R. Desai, and C. Wu. 2011. Observed variability of Lake Superior pCO2. Limnol. Oceanogr. 56: 775–786.

Bastviken, D., I. Sundgren, S. Natchimuthu, H. Reyier, and M. Gålfalk. 2015. Technical Note: Cost-efficient approaches to measure carbon dioxide (CO2) fluxes and concentrations in terrestrial and aquatic environments using mini loggers. Biogeosciences 12: 3849–3859.

Bockmon, E. E., and A. G. Dickson. 2015. An inter-laboratory comparison assessing the quality of seawater carbon dioxide measurements. Marine Chemistry 171: 36–43. doi:10.1016/j.marchem.2015.02.002.

Borges, A. V., F. Darchambeau, C. R. Teodoru, T. R. Marwick, F. Tamooh, N. Geeraert, F. O. Omengo, F. Guérin, T. Lambert, C. Morana, E. Okuku, and S. Bouillon. 2015. Globally significant greenhouse-gas emissions from African inland waters. Nature Geosci 8: 637–642.

Butman, D., and P. A. Raymond. 2011. Significant efflux of carbon dioxide from streams and rivers in the United States. Nature Geosci 4: 839–842. doi:10.1038/ngeo1294.

Cole, J. J., Y. T. Prairie, N. F. Caraco, W. H. McDowell, L. J. Tranvik, R. G. Striegl, C. M. Duarte, P. Kortelainen, J. A. Downing, J. J. Middelburg, and J. Melack. 2007. Plumbing the Global Carbon Cycle: Integrating Inland Waters into the Terrestrial Carbon Budget. Ecosystems 10: 172–185.

Accepted Article

This article is protected by copyright. All rights reserved.

DeGrandpre, M. D., T. R. Hammar, S. P. Smith, and F. L. Sayles. 1995. In situ measurements of seawater pCO2. Limnol. Oceanogr. 40: 969–975.

Dickson, A.G., Sabine, C.L. and J.R. Christian (Eds.). 2007. Guide to best practices for ocean CO2 measurements. PICES Special Publication 3, 191 pp.

Fietzek, P., B. Fiedler, T. Steinhoff, and A. Körtzinger. 2013. In situ Quality Assessment of a Novel Underwater pCO2 Sensor Based on Membrane Equilibration and NDIR Spectrometry. J. Atmos. Oceanic Technol. 31: 181–196. doi:10.1175/JTECH-D-13-00083.1.

Frankignoulle, M. 1988. Field measurements of air-sea CO2 exchange. Limnol. Oceanogr. 33: 313–322.

Frankignoulle, M., and A. V. Borges. 2001. Direct and Indirect pCO2 Measurements in a Wide Range of pCO2 and Salinity Values (The Scheldt Estuary). Aquatic Geochemistry 7: 267–273.

Friederich, G. E., P. G. Brewer, R. Herlien, and F. P. Chavez. 1995. Measurement of sea surface partial pressure of C02 from a moored buoy. Deep Sea Research Part I: Oceanographic Research Papers **42**: 1175–1186. doi:10.1016/0967-0637(95)00044-7.

Hales, B., and T. Takahashi. 2004. High-resolution biogeochemical investigation of the Ross Sea, Antarctica, during the AESOPS (U. S. JGOFS) Program. Global Biogeochem. Cycles 18: GB3006. doi:10.1029/2003GB002165.

Accepted Article

This article is protected by copyright. All rights reserved.

Hanson, P. C., D. L. Bade, S. R. Carpenter, and T. K. Kratz. 2003. Lake metabolism: Relationships with dissolved organic carbon and phosphorus. Limnol. Oceanogr. **48**: 1112–1119. doi:10.4319/lo.2003.48.3.1112

Hoppe, C. J. M., G. Langer, S. D. Rokitta, D. A. Wolf-Gladrow, and B. Rost. 2012. Implications of observed inconsistencies in carbonate chemistry measurements for ocean acidification studies. Biogeosciences 9: 2401–2405. doi:10.5194/bg-9-2401-2012

Hunt, C. W., J. E. Salisbury, and D. Vandemark. 2011. Contribution of non-carbonate anions to total alkalinity and overestimation of pCO2 in New England and New Brunswick rivers. Biogeosciences 8: 3069–3076.

Hunt, C. W., J. E. Salisbury, and D. Vandemark. 2013. CO2 Input Dynamics and Air–Sea Exchange in a Large New England Estuary. Estuaries and Coasts 37: 1078–1091.

Johnson, M. S., M. F. Billett, K. J. Dinsmore, M. Wallin, K. E. Dyson, and R. S. Jassal. 2010. Direct and continuous measurement of dissolved carbon dioxide in freshwater aquatic systems—method and applications. Ecohydrol. 3: 68–78.

Laruelle, G. G., R. Lauerwald, B. Pfeil, and P. Regnier. 2014. Regionalized global budget of the CO2 exchange at the air-water interface in continental shelf seas. Global Biogeochem. Cycles 28: 2014GB004832.

Accepted Article

This article is protected by copyright. All rights reserved.

Laruelle, G. G., R. Lauerwald, J. Rotschi, P. A. Raymond, J. Hartmann, and P. Regnier. 2015. Seasonal response of air–water CO2 exchange along the land–ocean aquatic continuum of the northeast North American coast. Biogeosciences 12: 1447–1458.

Lewis, E. 1980. The practical salinity scale 1978 and its antecedents. IEEE Journal of Oceanic Engineering 5: 3–8. doi:10.1109/JOE.1980.1145448

McDonald, C. P., E. G. Stets, R. G. Striegl, and D. Butman. 2013. Inorganic carbon loading as a primary driver of dissolved carbon dioxide concentrations in the lakes and reservoirs of the contiguous United States. Global Biogeochem. Cycles 27: 285–295. doi:10.1002/gbc.20032.

Newton, J.A., R.A. Feely, E. B. Jewett, P. Williamson and J. Mathis.
2015. Global Ocean Acidification Observing Network: Requirements and Governance Plan. Second Edition, GOA-ON, http://www.goa-on.org/docs/GOA-ON_plan_print.pdf.

Park, P. K. 1969. Oceanic CO_2 System: An Evaluation of Ten Methods of Investigation. Limnol. Oceanogr. 14: 179–186.

Raymond, P. A., N. F. Caraco, and J. J. Cole. 1997. Carbon dioxide concentration and atmospheric flux in the Hudson River. Estuaries 20: 381–390.

Accepted Article

This article is protected by copyright. All rights reserved.

Raymond, P. A., J. Hartmann, R. Lauerwald, S. Sobek, C. McDonald, M. Hoover, D. Butman, R. Striegl, E. Mayorga, C. Humborg, P. Kortelainen, H. Dürr, M. Meybeck, P. Ciais, and P. Guth. 2013. Global carbon dioxide emissions from inland waters. Nature 503: 355–359.

Signorini, S. R., A. Mannino, R. G. Najjar, M. A. M. Friedrichs, W.-J. Cai, J. Salisbury, Z. A. Wang, H. Thomas, and E. Shadwick. 2013. Surface ocean pCO2 seasonality and sea-air CO2 flux estimates for the North American east coast. J. Geophys. Res. Oceans 118: 5439–5460.

Takahashi, T. 1961. Carbon dioxide in the atmosphere and in Atlantic Ocean water. J. Geophys. Res. 66: 477–494. doi:10.1029/JZ066i002p00477.

Vandemark, D., J. E. Salisbury, C. W. Hunt, S. M. Shellito, J. D. Irish, W. R. McGillis, C. L. Sabine, and S. M. Maenner. 2011. Temporal and spatial dynamics of CO2 air-sea flux in the Gulf of Maine. J. Geophys. Res. 116: C01012.

Wang, Z. A., D. J. Bienvenu, P. J. Mann, K. A. Hoering, J. R. Poulsen, R. G. M. Spencer, and R. M. Holmes. 2013. Inorganic carbon speciation and fluxes in the Congo River. Geophys. Res. Lett. 40: 511–516.

Wanninkhof, R., and K. Thoning. 1993. Measurement of fugacity of CO2 in surface water using continuous and discrete sampling methods. Marine Chemistry 44: 189–204.

Accepted Article

This article is protected by copyright. All rights reserved.

Weiss. 1981. Determinations of carbon dioxide and methane by dual catalyst flame ionization chromatography and nitrous oxide by electron capture chromatography. Determinations of Carbon-Dioxide and Methane by Dual Catalyst Flame Ionization Chromatography and Nitrous-Oxide by Electron-Capture Chromatography 19: 611–616.

Yasuda, T., S. Yonemura, and A. Tani. 2012. Comparison of the Characteristics of Small Commercial NDIR CO2 Sensor Models and Development of a Portable CO2 Measurement Device. Sensors 12: 3641–3655. doi:10.3390/s120303641

Accepted Article

This article is protected by copyright. All rights reserved.

Acknowledgements

Associate Editor Michael Degrandpre, reviewer Wiley Evans, and one anonymous reviewer provided essential criticism and feedback which greatly helped shape this work. Lauren Koenig provided a thoughtful review of an early version of this paper. Funding for this work was provided by NOAA Award NA15NOS0120155, NOAA/NERACOOS Award A002004, and EPSCoR Ecosystems and Society Award EPS-1101245.

Accepted Article

This article is protected by copyright. All rights reserved.

Figure Legends

Figure 1. Panel A- SIPCO2 sensor design. A components list is provided in the Supplementary Material. Panel B- the prototype SIPCO2 sensor deployed in the Lamprey River, New Hampshire USA.

Figure 2. Laboratory SIPCO2 sensor evaluation. Top panel- timeseries plot of SIPCO2 and validation system pCO_2 measurements. Difficulties with the K-30 CO_2 sensor logging software, which reset at the end of each day, resulted in the data gaps shown. Bottom panel- scatterplot of SIPCO2 pCO_2 readings against validation system pCO_2 readings, including two CO_2 additions (green points) and excluding CO_2 additions (black points).

Figure 3. Comparison data collected at the UNH Coastal Marine Lab. Top panel: time series of pCO_2 readings from SIPCO2 and validation systems. Data gaps in this panel are due to the removal of data when the validation system equilibrator was clogged. Bottom panel: time series of sensor offsets, with the mean offset from the Laboratory Evaluation shown as a solid line. Offsets were calculated as the difference between SIPCO2 and validation system measurements.

Figure 4. Corrected comparison data collected at the UNH Coastal Marine Lab. Top panel: time series of corrected SIPCO2 sensor and validation system readings. The SIPCO2 correction was derived from the Laboratory Evaluation results (Equation 3) . Bottom panel: time series of sensor offsets, with the mean offset from the Coastal Laboratory evaluation (-5 µatm) shown as a solid line. Linear regression of the corrected CML SIPCO2 sensor data against validation

Accepted Article

This article is protected by copyright. All rights reserved.

system readings results in an equation of $pCO_{2\ SIPCO2} = 1.08*pCO_{2\ validation} - 30.8$, with a r^2 of 0.969 and $p<<0.001$.

Figure 5. Comparison of xCO_2 response between a Li-cor LI840 NDIR and a K-30 NDIR of the same model used in the SIPCO2 sensor. Standard deviation error bars in both the x- and y-directions are too small to appear in the plot. The dashed line indicates a 1:1 response, while the solid line shows the regression line between LI840 and K-30 detectors.

Figure 6. Change in K-30 NDIR readings of a constant sample gas stream with varying temperature. Changes in UHP N_2 gas (0 ppm xCO_2) are shown in blue, while those of a 515 ppm $CO2/N_2$ mixture are shown in red. The K-30 NDIR was calibrated at 20°C. Results from Yasuda et al. 2012 are shown in green, also for a K-30 NDIR calibrated at 20°C. The black line shows a logarithmic regression of the combined UHP N_2 and 515 ppm $CO2/N_2$ data.

Figure 7. Response of a K-30 NDIR detector to humidity change produced by a Li-cor LI-610 dew point generator. Blue points show changes in xCO2 readings for UHP N_2 gas (0 ppm xCO_2), while red points show xCO2 changes for a 515 ppm $CO2/N_2$ mixture. Second-order polynomial regression lines and equations are shown in blue and red for the UHP N_2 gas and 515 ppm $CO2/N_2$ mixture, respectively.

Accepted Article

This article is protected by copyright. All rights reserved.

Accepted Article

Table 1- Aquatic CO_2 sensors and their performance characteristics.

Manufacturer/Sensor	Measurement Method	Range of difference from standard system (mean difference)	Standard Deviation Range	Citation
Contros Hydro-C	pumped membrane equilibration, NDIR detection	-16 to +96 µatm	+/- 17 to 25 µatm	ACT 2010a
Pro-Oceanus CO_2-Pro	pumped membrane equilibration, NDIR detection	+9 µatm	+/- 14 µatm	ACT 2010b
Vaisala CARBOCAP (modified)	passive membrane equilibration, NDIR detection	+5 to +881 ppm[1]	not reported	Johnson et al. 2010
Sunburst SAMI-CO2	passive membrane equilibration, reagent-based colorimetry	+18 to +40 µatm	+/- 9 to 40 µatm	ACT 2010c
PMEL/Batelle MAPCO2	bubble equilibration, NDIR detection	-12 to +3 µatm	+/- 8 to 30 µatm	ACT 2010d
This study- before characterization	pumped air equilibration, NDIR detection	+7 to +65 µatm[2]	+ / - 6 µatm	This study
This study- after characterization	pumped air equilibration, NDIR detection	-26 to +30 µatm[3]	+ / - 6 µatm	This study

[1]Converted from mg/L, assuming 0°C and 1.01325 bar pressure

[2]SIPCO2 CML data without Laboratory Calibration applied

[3]SIPCO2 CML data with Laboratory Calibration applied

This article is protected by copyright. All rights reserved.

Table 2- Offset and linear regression results of the Laboratory Evaluation of the SIPCO2 sensor.

	With Peaks	Without Peaks
Off_{mean} (µatm)	30.2 (±76.7)	42.7 (±14.2)
Slope	0.88	1.03
Intercept	105	22
R^2	0.92	0.99

Table 3- Summary of hydrographic conditions and pCO_2 observations from the Coastal Marine Lab evaluation. Min is the minimum measurement during the evaluation, Max is the maximum measurement observed, Std is the standard deviation of the measurement during the evaluation (n=2,539 hourly means).

	Mean	Median	Min	Max	Std
Salinity	29.95	30.45	22.31	32.28	1.87
Water temperature	4.31	4.85	-0.75	10.39	2.93
Dissolved Oxygen (µmol l-1)	345	338	269	433	33
Validation pCO2	402	399	338	472	27
K-30 pCO2	431	430	360	501	30

Table 4- Offsets and regressions of uncorrected and corrected data from the CML SIPCO2 sensor test. Offsets were calculated as $pCO_{2\ SIPCO2}$ - $pCO_{2\ validation}$. The Laboratory Offset applied was 42.7 µatm (without peaks). The Laboratory Calibration applied to the data was that

This article is protected by copyright. All rights reserved.

derived from the linear regression of data from the initial Laboratory Evaluation: $pCO_{2\ SIPCO2\ corrected} = (pCO_{2\ SIPCO2\ measured} - 22)/1.03$.

Accepted Article

	SIPCO2 Uncorrected Data	SIPCO2 Laboratory Offset Applied	SIPCO2 Laboratory Calibration Applied
Off_{mean} (µatm)	29 (±6)	-13.8 (±6)	-5 (±5)
Slope	1.08	1.04	1.04
Intercept	-1.9	-23.5	-23
R^2	0.97	0.97	0.97

This article is protected by copyright. All rights reserved.

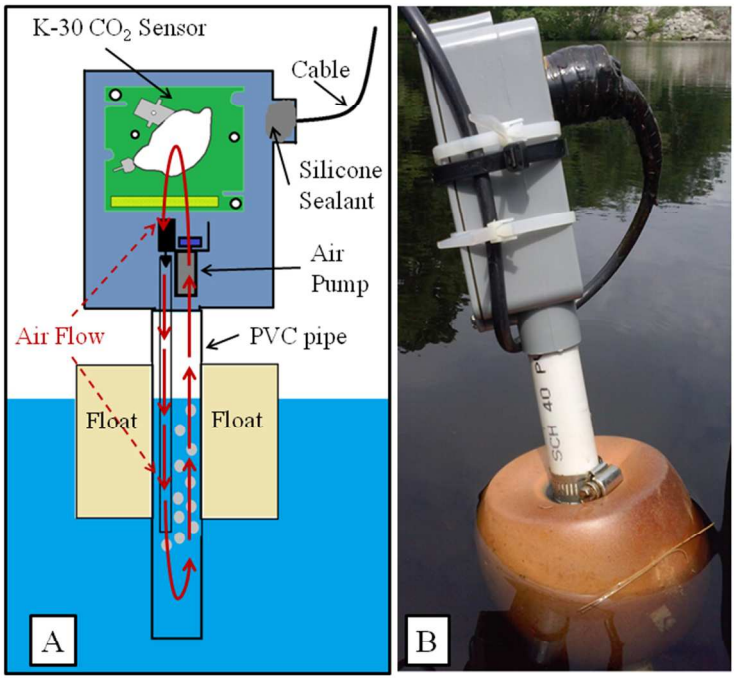

Figure 1. Panel A- SIPCO2 sensor design. A components list is provided in the Supplementary Material. Panel B- the prototype SIPCO2 sensor deployed in the Lamprey River, New Hampshire USA.

254x190mm (96 x 96 DPI)

Accep

This article is protected by copyright. All rights reserved.

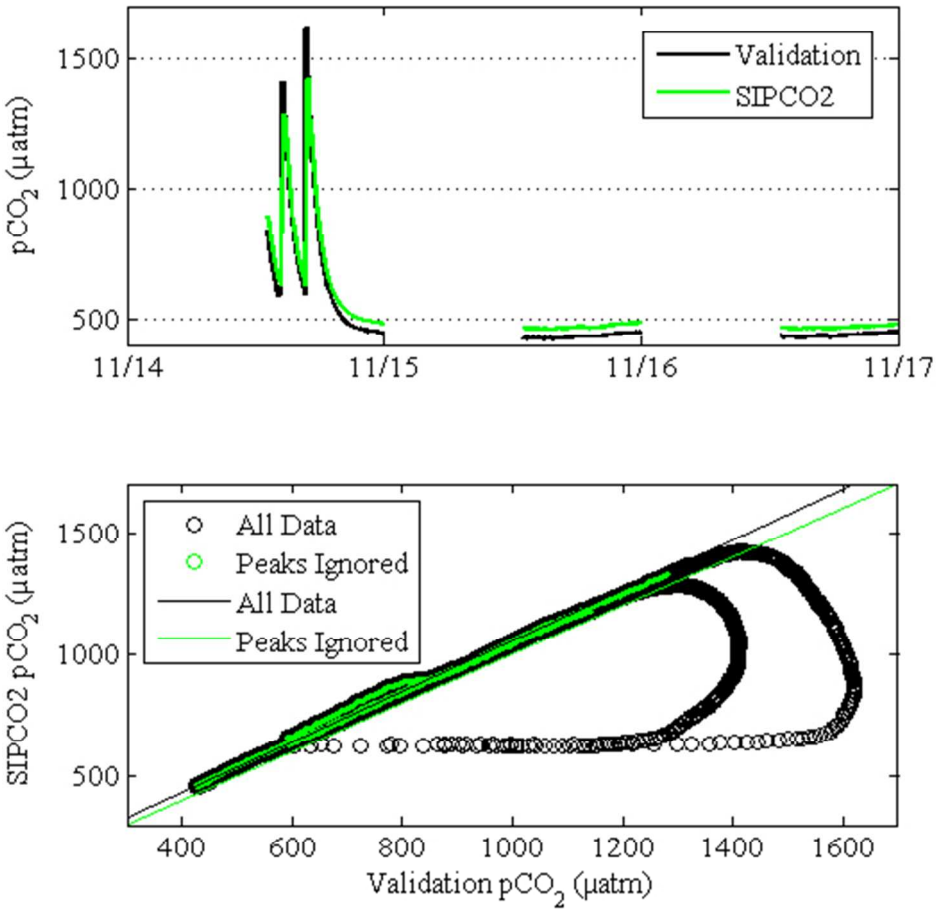

Figure 2. Laboratory SIPCO2 sensor evaluation. Top panel- timeseries plot of SIPCO2 and validation system pCO2 measurements. Difficulties with the K-30 CO2 sensor logging software, which reset at the end of each day, resulted in the data gaps shown. Bottom panel- scatterplot of SIPCO2 pCO2 readings against validation system pCO2 readings, including two CO2 additions (green points) and excluding CO2 additions (black points).

148x150mm (96 x 96 DPI)

This article is protected by copyright. All rights reserved.

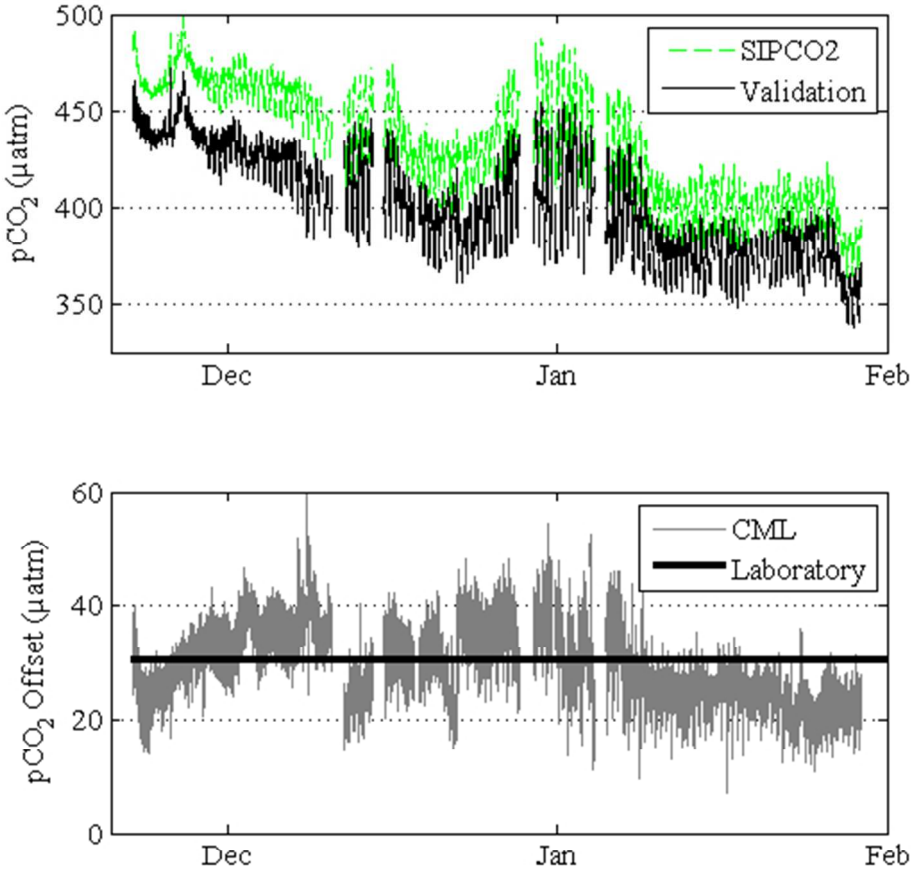

Figure 3. Comparison data collected at the UNH Coastal Marine Lab. Top panel: time series of pCO2 readings from SIPCO2 and validation systems. Data gaps in this panel are due to the removal of data when the validation system equilibrator was clogged. Bottom panel: time series of sensor offsets, with the mean offset from the Laboratory Evaluation shown as a solid line. Offsets were calculated as the difference between SIPCO2 and validation system measurements.

148x150mm (96 x 96 DPI)

This article is protected by copyright. All rights reserved.

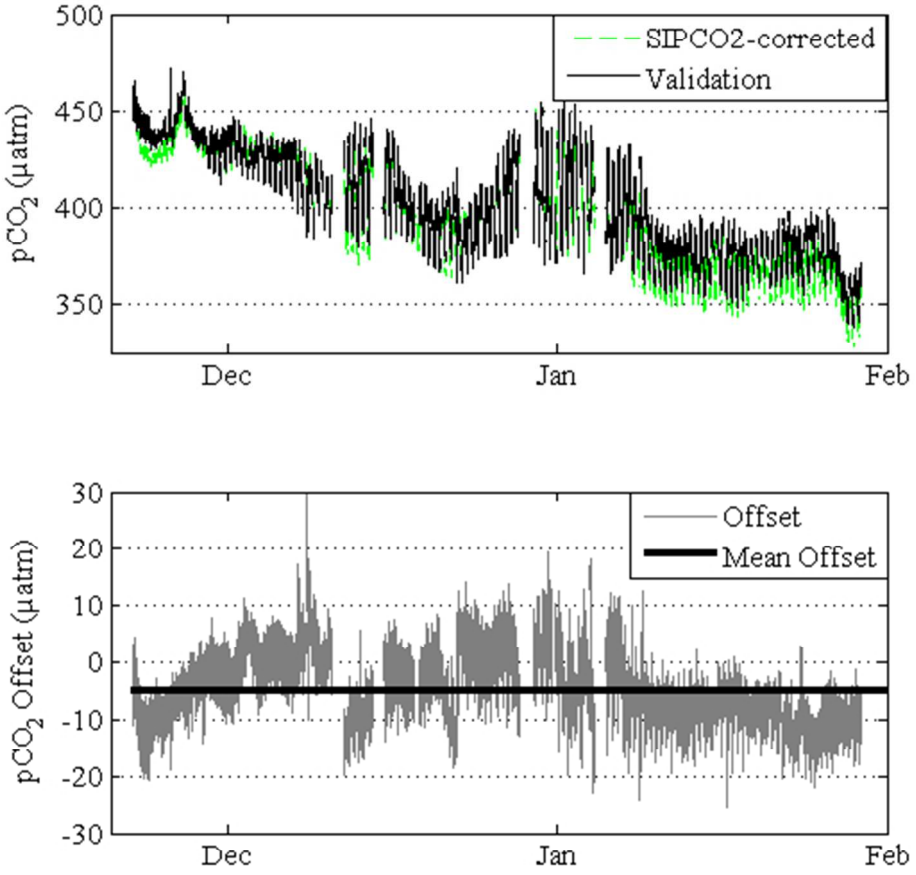

Figure 4. Corrected comparison data collected at the UNH Coastal Marine Lab. Top panel: time series of corrected SIPCO2 sensor and validation system readings. The SIPCO2 correction was derived from the Laboratory Evaluation results (Equation 3) . Bottom panel: time series of sensor offsets, with the mean offset from the Coastal Laboratory evaluation (-5 µatm) shown as a solid line. Linear regression of the corrected CML SIPCO2 sensor data against validation system readings results in an equation of pCO2 SIPCO2 = 1.08*pCO2 validation - 30.8, with a r2 of 0.969 and p<<0.001.

148x150mm (96 x 96 DPI)

This article is protected by copyright. All rights reserved.

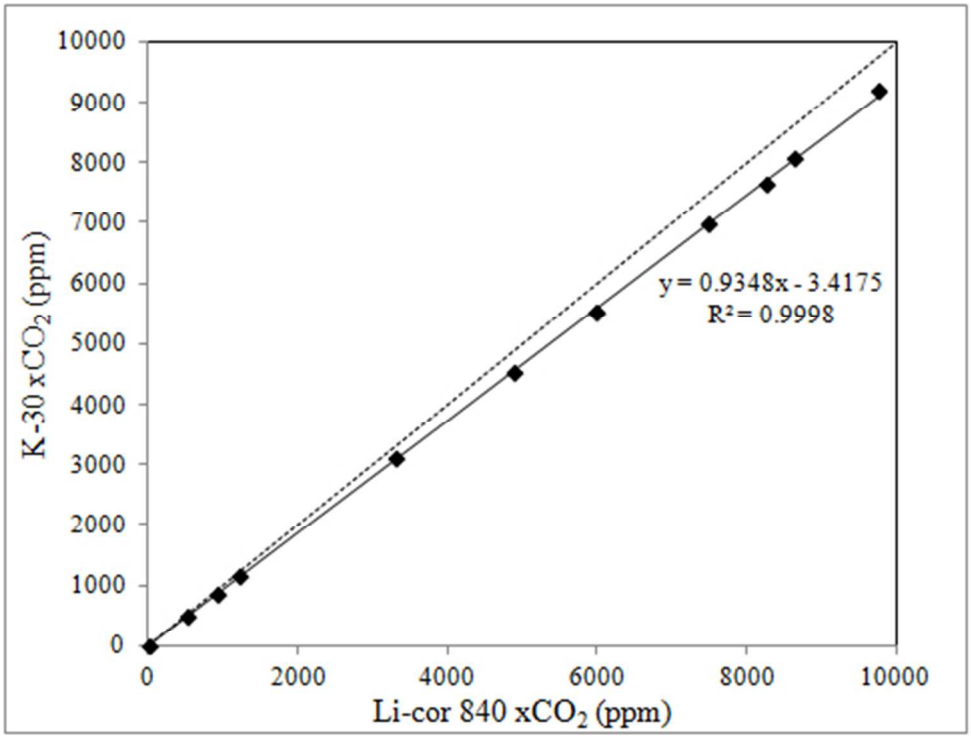

Figure 5. Comparison of xCO2 response between a Li-cor LI840 NDIR and a K-30 NDIR of the same model used in the SIPCO2 sensor. Standard deviation error bars in both the x- and y-directions are too small to appear in the plot. The dashed line indicates a 1:1 response, while the solid line shows the regression line between LI840 and K-30 detectors.

85x64mm (144 x 144 DPI)

Accep

This article is protected by copyright. All rights reserved.

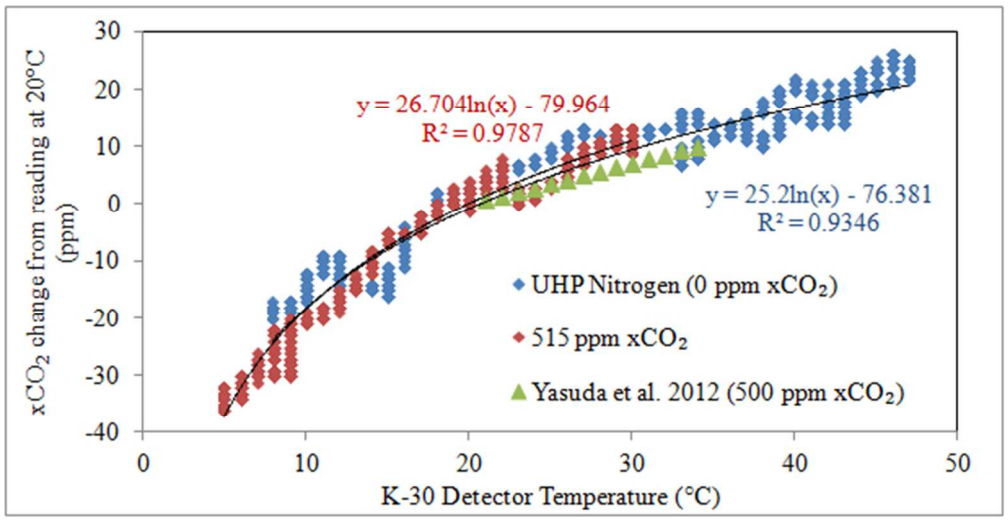

Figure 6. Change in K-30 NDIR readings of a constant sample gas stream with varying temperature. Changes in UHP N2 gas (0 ppm xCO2) are shown in blue, while those of a 515 ppm CO2/N2 mixture are shown in red. The K-30 NDIR was calibrated at 20°C. Results from Yasuda et al. 2012 are shown in green, also for a K-30 NDIR calibrated at 20°C. The black line shows a logarithmic regression of the combined UHP N2 and 515 ppm CO2/N2 data.

108x55mm (144 x 144 DPI)

Accepte

This article is protected by copyright. All rights reserved.

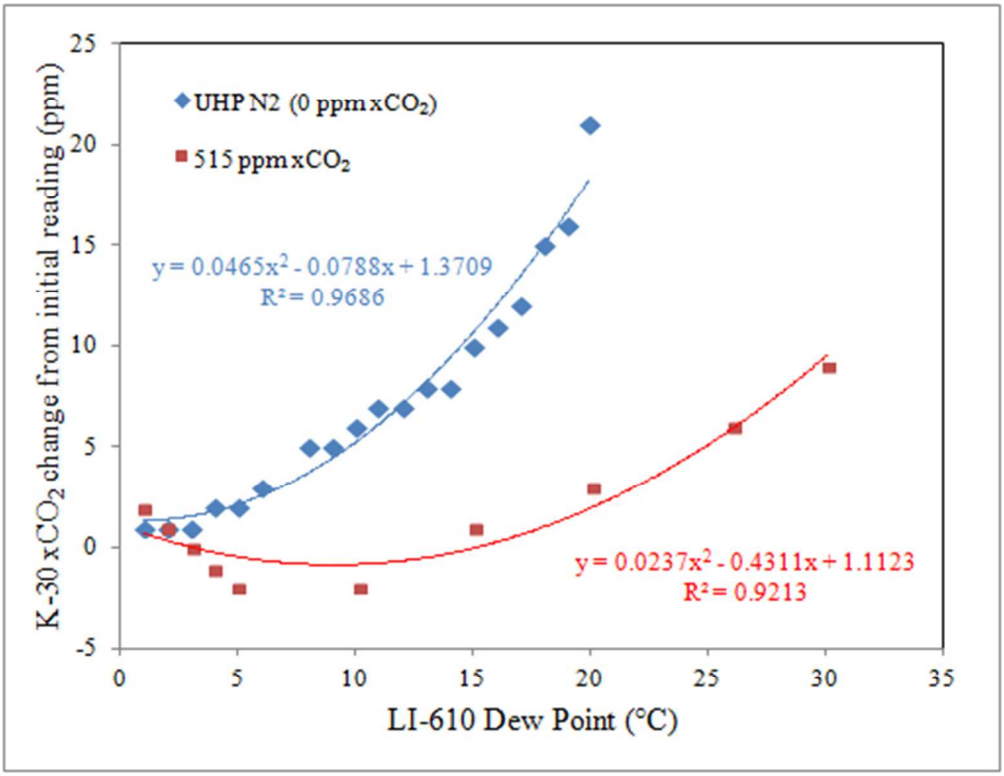

Figure 7. Response of a K-30 NDIR detector to humidity change produced by a Li-cor LI-610 dew point generator. Blue points show changes in xCO2 readings for UHP N2 gas (0 ppm xCO2), while red points show xCO2 changes for a 515 ppm CO2/N2 mixture. Second-order polynomial regression lines and equations are shown in blue and red for the UHP N2 gas and 515 ppm CO2/N2 mixture, respectively.

90x69mm (144 x 144 DPI)

Acce

This article is protected by copyright. All rights reserved.

Accepted Article

Supplementary Material

SIPCO2 Sensor Assembly

*Note that dimensions and measurements in these instructions are provided in Standard units, as opposed to metric, as those are the units used by the suppliers. These instructions do not represent an endorsement of the suppliers listed, but simply a reference point for those building a sensor.

Materials:

- K-30 ASCII CO_2 sensor (http://www.co2meter.com/collections/co2-sensors/products/k-30-ascii-co2-sensor)
- Solderless headers (https://www.sparkfun.com/search/results?term=10527)
- 20 or 22 AWG wire (red, black, white, and green) (http://www.mcmaster.com/#standard-electrical-wire/=wld3qw)
- Heat-shrink for 20 or 22 AWG wire (http://www.mcmaster.com/#heat-shrink-tubing/=wld4sb)
- Male and female Snap-Plug Terminals (http://www.mcmaster.com/#standard-electrical-wire-terminals/=wld678)
- 6 wire bundled direct-bury cables (http://www.mcmaster.com/#standard-electrical-wire/=wld6zs)
- Brushless Pump- KNF Neuberger MPU3671-NMP05
- 1/8-inch tubing to fit Brushless Pump (i.e. Bev-a-Line IV)
- Extra PVC pipe for deeper down-stem (3/4-inch OD)
- Thick-Wall Dark Gray PVC Thread-One-End Pipe Nipple, ¾ Pipe Size X 12-inch Length Schedule 80 (http://www.mcmaster.com/#catalog/121/94/=x4ztef)

This article is protected by copyright. All rights reserved.

Accepted Article

- Rigid PVC Conduit Fitting, Coupling, ¾ Trade Size (http://www.mcmaster.com/#catalog/121/865/=x4ztqs)
- Rigid PVC Conduit Fitting, Female Adapter, ¾ Trade Size (http://www.mcmaster.com/#catalog/121/865/=x4zsvj)
- Rigid PVC Conduit Access Port, 90 Degree elbow, ¾ Trade Size (http://www.mcmaster.com/#catalog/121/865/=x4zsfa)
- Small plastic funnel
- Silicone sealant
- Zip-ties
- Adhesive zip-tie mounts

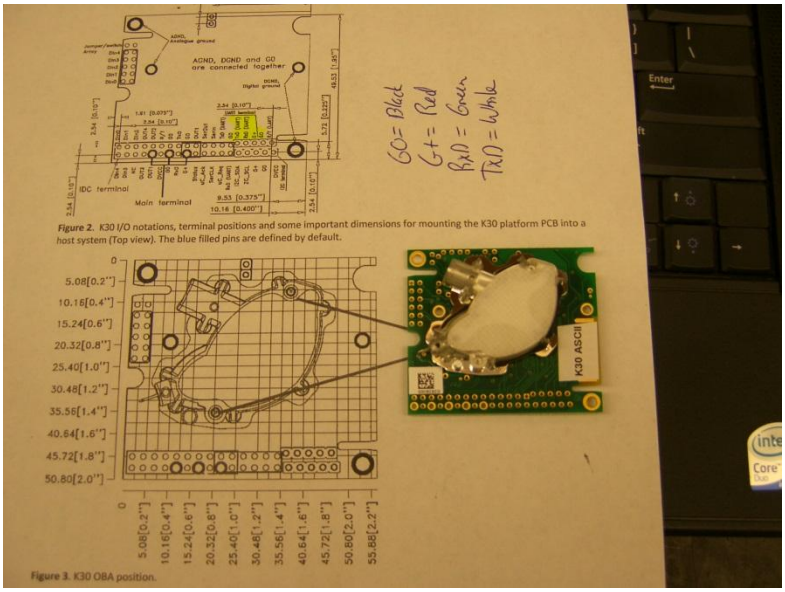

Figure S1 – K30 ASCII sensor out of the box: unwired, no jumper in place

Directions:

1. Wire the Sensor:
    a. First prepare the wires:
        i. Cut 3 inches of 22 AWG wire from each: red, black, white, green

This article is protected by copyright. All rights reserved.

ii. Strip each end leaving about ¼ to 3/8 inches of bare wire at each end.

iii. Solder each to a solderless header (this can be done with the header already inserted into the proper port, if desired).

iv. Heat-shrink around the solderless pin

v. Connect a male removable splice to the other end of the 22 AWG wire (Figure S2).

Figure S2 – Prepared wires with solderless connectors ready to be mounted onto CO_2 sensor

b. If not done already (see step a.iii) connect the prepared wires to the proper port (see Figure S3)

This article is protected by copyright. All rights reserved.

Accepted Article

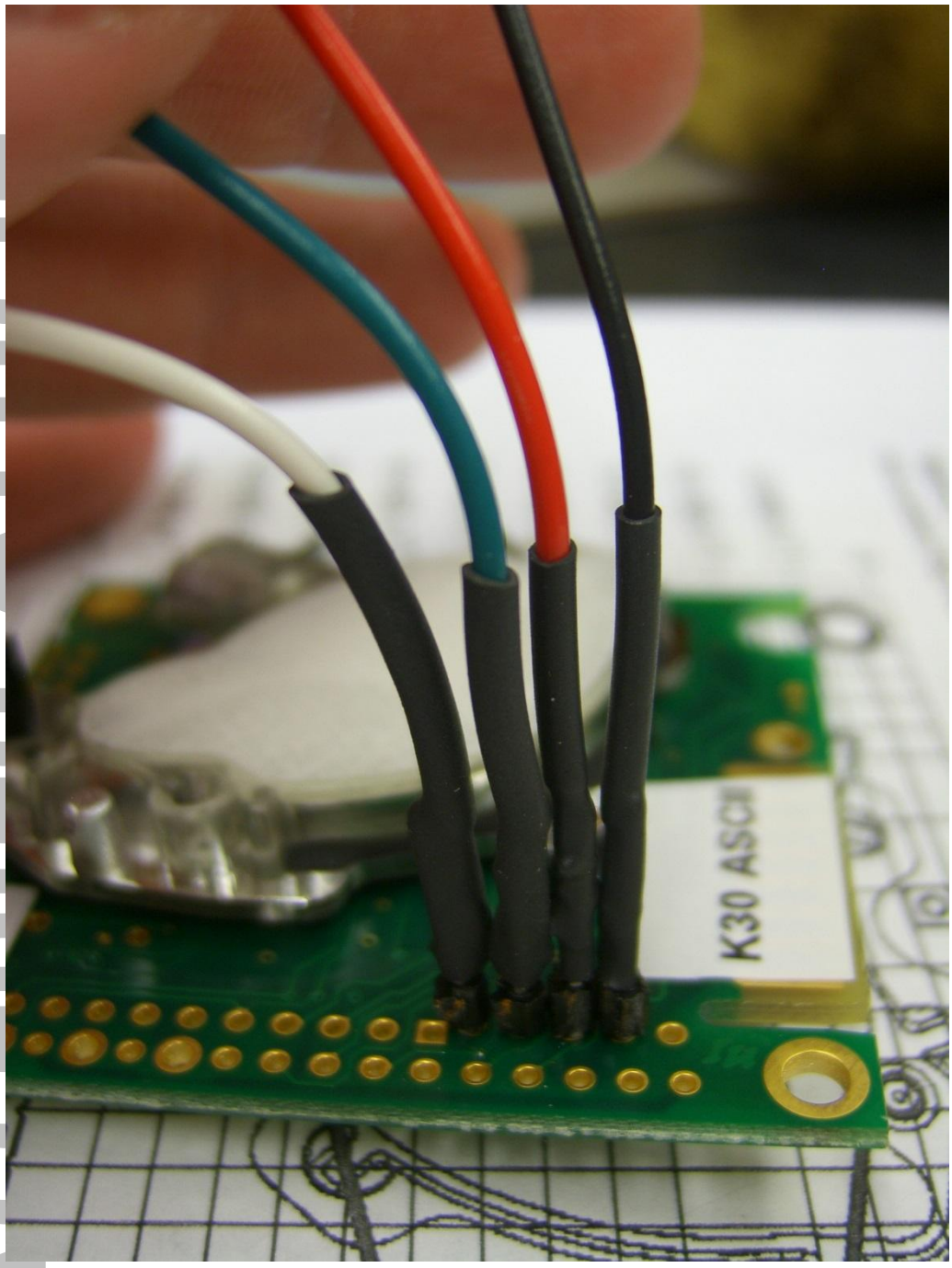

Figure S3 – Power and communication wiring installed on CO_2 sensor

c. Solder the jumper on the underside of the board (Figures S4 and S5), being careful not to bride any two pins or connectors with solder.

This article is protected by copyright. All rights reserved.

Accepted Article

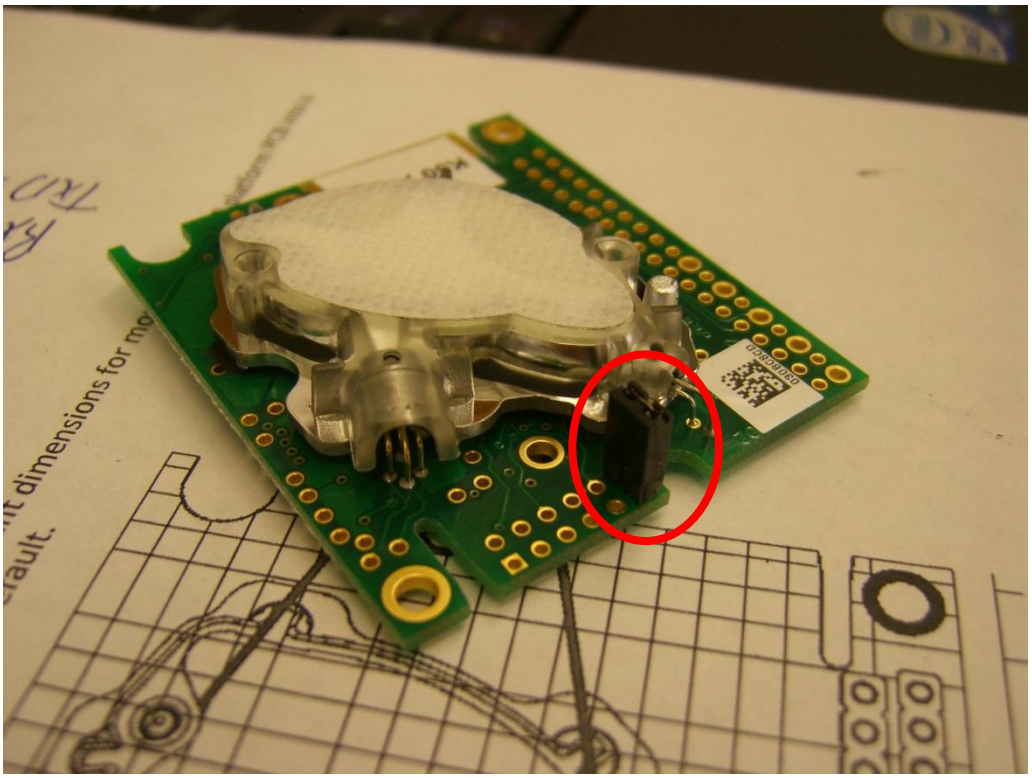

Figure S4 – Jumper (circled) shown in correct location, right side up.

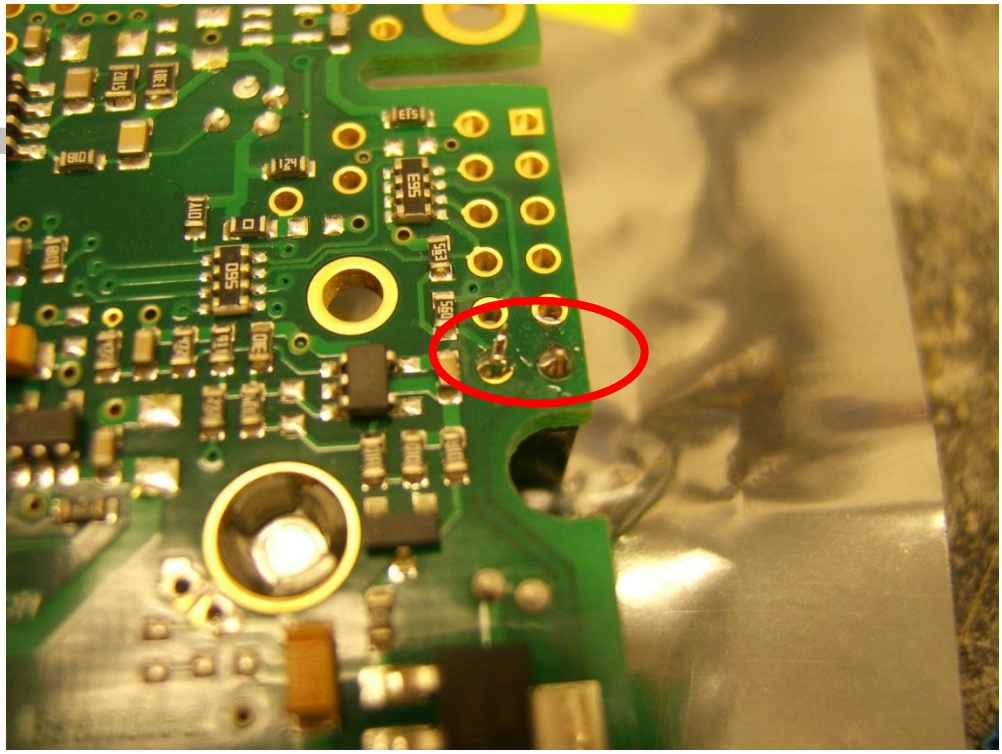

This article is protected by copyright. All rights reserved.

Figure S5 – Jumper pins (circled) soldered on the under-side of the CO_2 sensor.

2. Assembling the CO_2 housing
   a. Cut two sections of the white PVC pipe, the first about 3 inches (this will be attached to the junction box), and the second about 2-3 feet depending on your field installation needs.
   b. Prep any joints by priming the inside and outside of the sections to be joined (Figure S6)
   c. PVC cement should be used to attach the joining the sections (Figure S7)

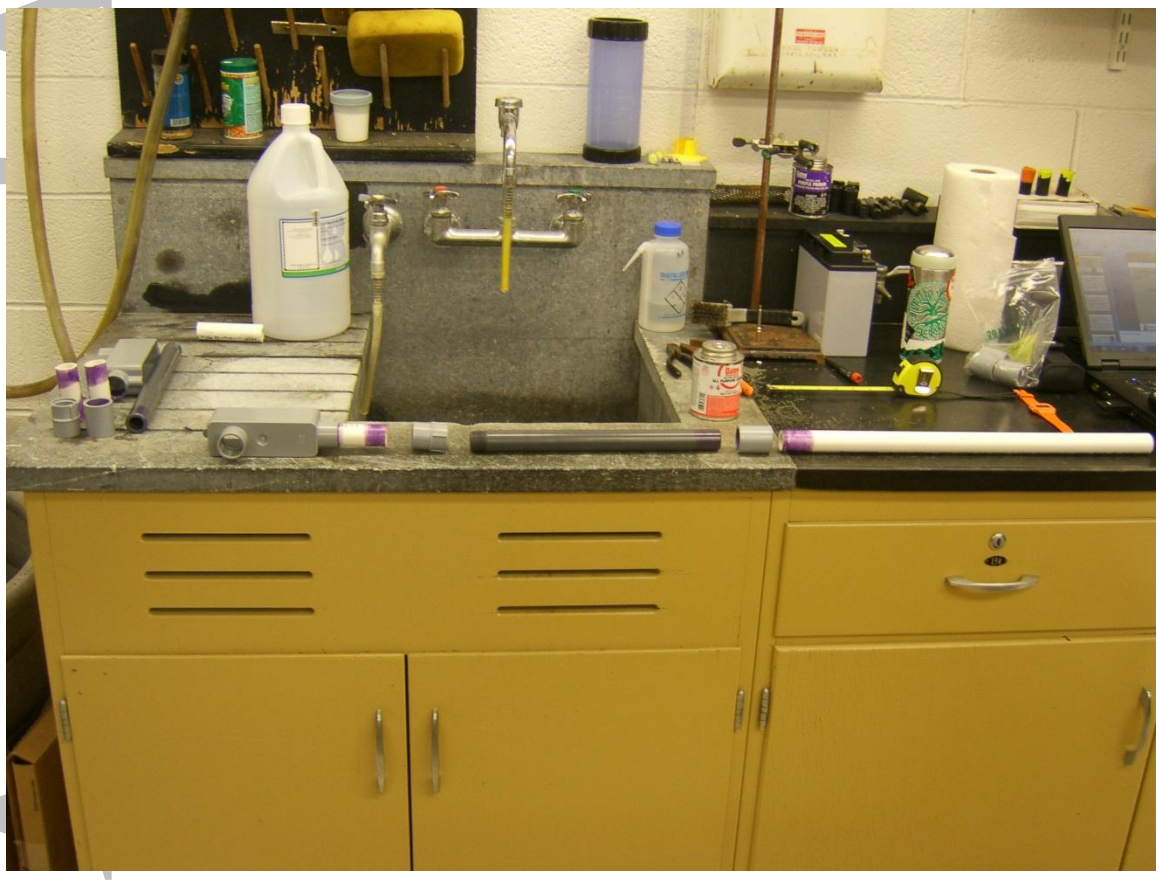

Figure S6 – Sections of housing prepped for cement

This article is protected by copyright. All rights reserved.

Accepted Article

Figure S7 – Housing with all joints connected

d. Drill out flow-through ports/holes on the bottom of the down-stem beginning about 3-4 inches from the bottom (Figure 8)

This article is protected by copyright. All rights reserved.

Accepted Article

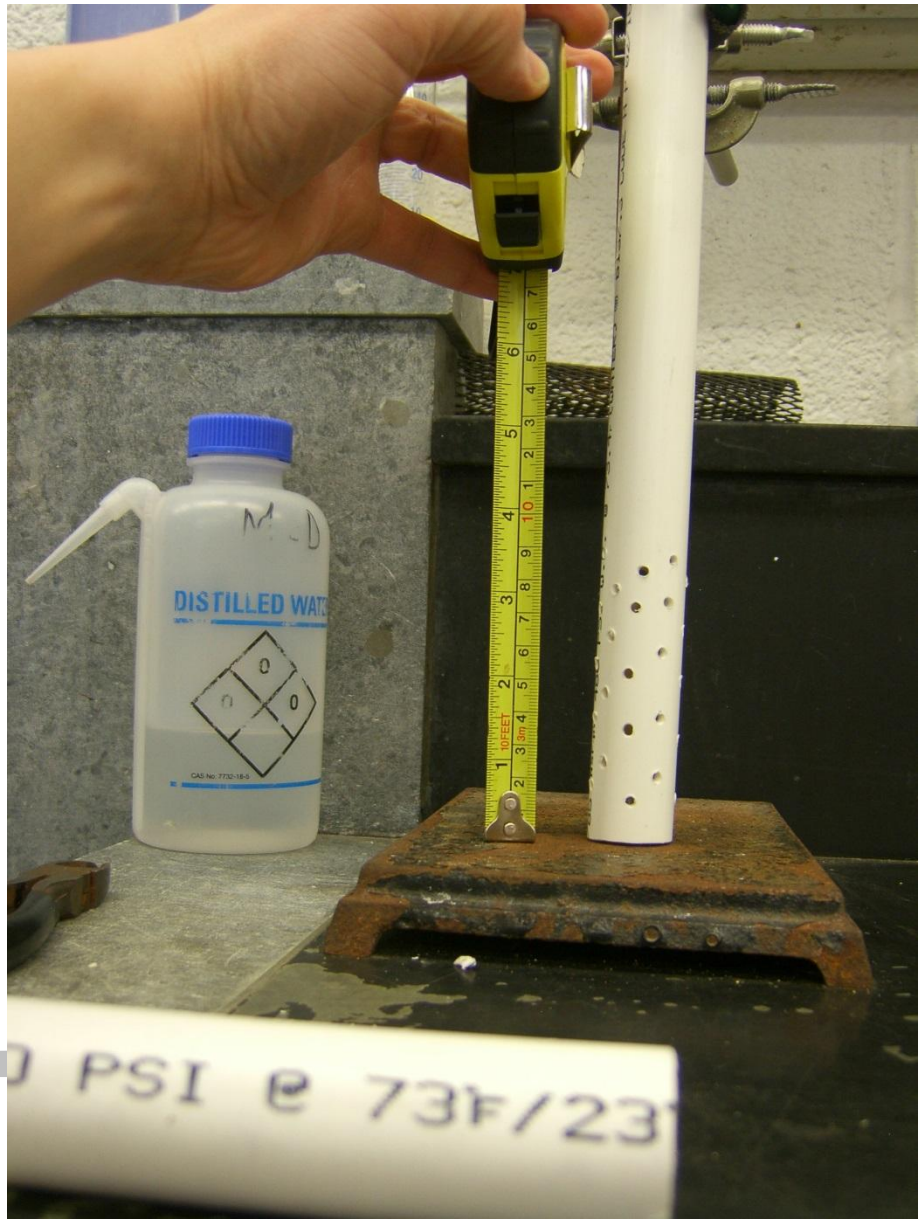

Figure S8 – Flow-through holes drilled in the bottom of the down-stem.

3. Prep the field-cable wiring:
   a. Strip back 6-8 inches of the coaxial sheath (Figure S9A and S9B)
   b. Strip about ¼ inch from each individual wire and crimp on removable splices (Figure 10):
      i. Red – Female

This article is protected by copyright. All rights reserved.

ii. Black – Female

iii. White – Female

iv. Green – Female

v. Blue – Female

vi. Yellow – Male (this may help in not confusing power wires for pump)

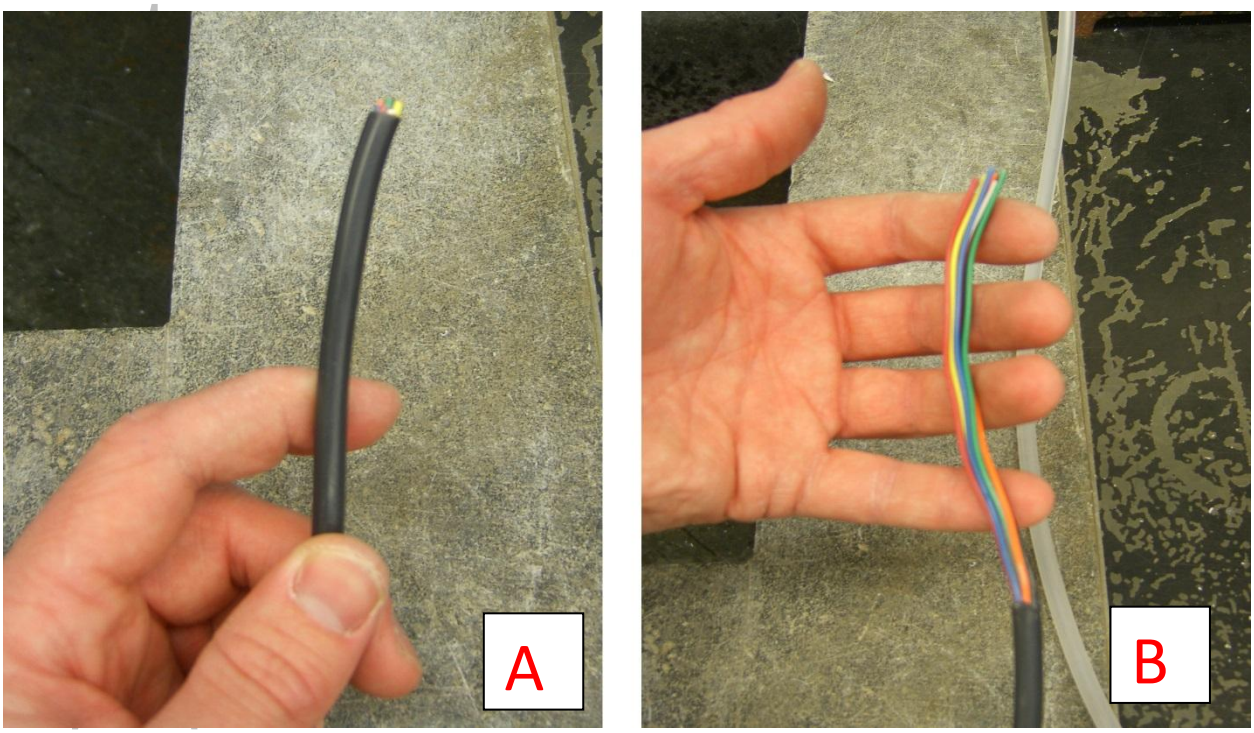

Figure S9 – Strip back coaxial sheathing about 6-8 inches

Accepted Article

This article is protected by copyright. All rights reserved.

Accepted Article

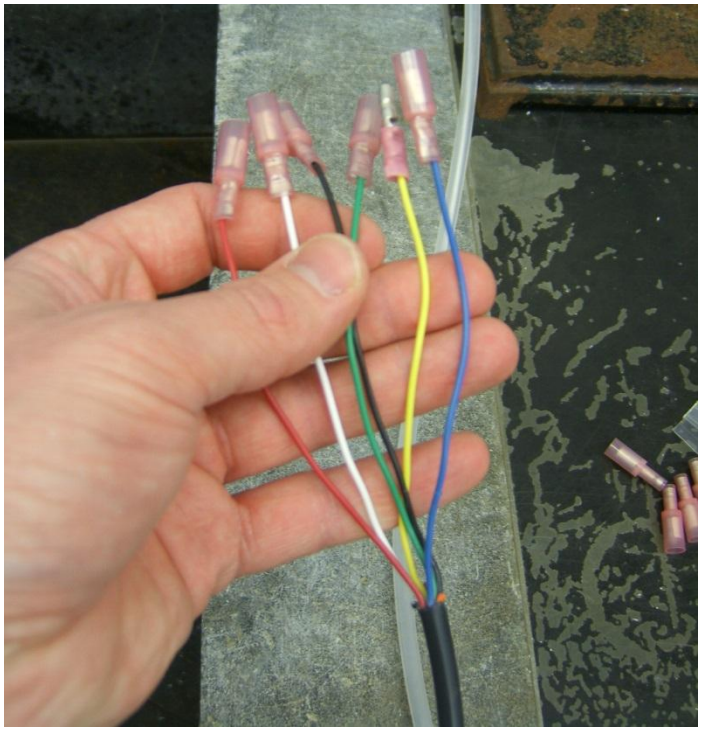

Figure S10 – Crimp on appropriate removable-splices to each wire

4. Prep the pump:
   a. Crimp on a male splice to the red and a female splice to the black wire on the pump. Connect a length of flexible tubing that will reach about ½ inch from the bottom of the down-stem when the pump is resting in the small funnel inside the junction box (shown in Figure 11).

This article is protected by copyright. All rights reserved.

Accepted Article

Figure S11 – Pump with splices crimped on, and flex-tubing cut to length. The tubing threads though a funnel inside the junction box, and the pump will sit in the funnel.

5. Bring the field-cable into the junction box:
    a. Thread the field cable with splice-connector ends into the upper junction of the box (Figure S12A). Use adhesive zip tie mounts (shown in Figure S12B) to secure the cable in place both outside and inside the box. Use two mounts inside if necessary

This article is protected by copyright. All rights reserved.

to keep the cable snug to the inner wall.

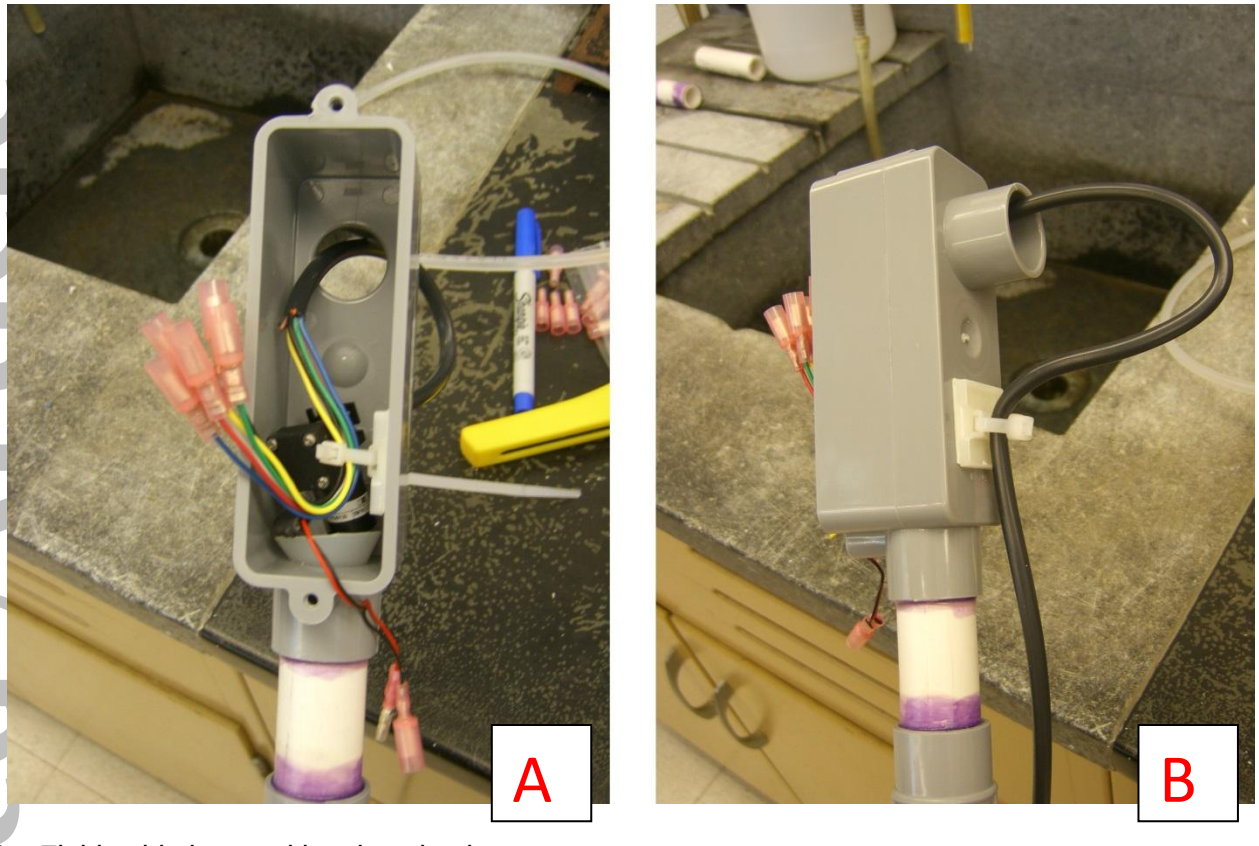

Figure S12 – Field cable inserted into junction box

b. Connect each field cable wire splice to the appropriate CO_2 sensor wire splice or pump power wire splice (Figure S13).

Accepted Article

This article is protected by copyright. All rights reserved.

Figure S13 – Field Cable is connected to the CO_2 sensor and pump.

6. Seal the upper junction of the box with silicone (Figure S14). This process should be done over the course of 3 days. Make the first coat starting from the outside of the box. This coat should not be too thick, to allow for proper curing. Once the first coat has cured, the second coat should be applied from the inside of the box, being sure to cover any holes from the first coat. When the second coat has cured, one final coat can be applied from the outside of the box, again, ensuring any holes present in the silicone are filled.

Accepted Article

This article is protected by copyright. All rights reserved.

Figure S14 – The first coat of silicone sealant, applied from the outside of the box.

7. Calibrate the CO_2 Sensor before deployment:
   a. Download DAS onto your computer from the CO_2 meter website: http://www.co2meter.com/pages/downloads
   b. Remove the jumper from the CO_2 sensor to allow the DAS software to work with the CO_2 meter.
   c. Obtain a nitrogen gas standard (0 ppm CO_2) and a 400 ppm CO_2 standard. Connect a piece of Tygon (or similar) flexible tubing to each regulator and put the end of the tubing into a Ziploc bag. Connect the CO_2 meter to a computer using a USB test cable ordered with the CO_2 meter, and place this in the Ziploc as well. Seal the bag

Accepted

This article is protected by copyright. All rights reserved.

as well as possible, leaving a small gap around the tubing and data cable for gas to escape (Figure S15).

Figure S15 – CO_2 meter inside Ziplock bag with USB cable and standard gas tube

d. With the CO_2 meter sealed in the bag, turn the pure nitrogen gas regulator on, letting the bag fill for a few minutes, and letting the CO_2 readings stabilize. Once stable, select the "Calibrate" option with the nitrogen box selected. The reading should shift to 0 (+/- 1 or 2). If drifting, Calibrate again.

e. When satisfied with the 0 ppm calibration, turn the nitrogen gas off and flow the 400 ppm CO_2 standard few minutes. Once stable, with the 400ppm box selected, hit the

This article is protected by copyright. All rights reserved.

"Calibrate" option. Again, make sure the sensor reading does not drift, calibrating again until satisfied.

f. Stop logging data, disconnect from the computer and replace the jumper on the CO_2 meter.

g. With the jumper replaced, the sensor should transmit a CO_2 reading every two seconds to a computer or data logger.

Accepted Article

This article is protected by copyright. All rights reserved.